Available online at www.sciencedirect.com
ScienceDirect
Solar Energy 82 (2008) 272–285
SOLAR ENERGY
www.elsevier.com/locate/solener

REST2: High-performance solar radiation model for cloudless-sky irradiance, illuminance, and photosynthetically active radiation – Validation with a benchmark dataset

Christian A. Gueymard [1]

Solar Consulting Services, P.O. Box 392, Colebrook, NH 03576, USA

Received 26 August 2006; received in revised form 24 February 2007; accepted 22 April 2007
Available online 24 May 2007

Communicated by: Associate Editor David Renne

Abstract

REST2, a high-performance model to predict cloudless-sky broadband irradiance, illuminance and photosynthetically active radiation (PAR) from atmospheric data, is presented. Its derivation uses the same two-band scheme as in the previous CPCR2 model, but with numerous improvements. Great attention is devoted to precisely account for the effect of aerosols, in particular.

Detailed research-class measurements from Billings, OK are used to assess the performance of the model for the prediction of direct, diffuse and global broadband irradiance. These measurements were made in May 2003 during a sophisticated radiative closure experiment, which involved the best radiometric instrumentation currently available and many ancillary instruments. As a whole, these exceptional measurements constitute the only known modern benchmark dataset made specifically to test the intrinsic performance of radiation models. Using this dataset as reference, it is shown that REST2 performs better than CPCR2 for irradiance, illuminance or PAR predictions. The availability of the turbidity data required by REST2 or other similar models is also discussed, as well as the effect that turbidity has on each component of broadband irradiance, PAR irradiance and illuminance, and on the diffuse/global PAR ratio.

Keywords: Solar radiation; Irradiance; Illuminance; Photosynthetically active radiation; Radiation model; Validation; Radiative closure; Performance assessment; Radiometry; Diffuse radiation; Turbidity; Aerosols

1. Introduction

Many solar energy applications require an evaluation of the radiation input to solar energy systems from meteorological data. Cloudless-sky data are particularly important because they correspond to the maximum output of solar systems. They are also needed for the design and sizing of solar systems or air conditioning equipment in buildings or vehicles.

Recent studies (Gueymard, 2003b,a) have shown that the accuracy of many broadband models of the literature was not always satisfactory, primarily because of the extreme simplicity of their parameterizations. These studies also introduced two high-performance models to predict direct irradiance. However, in most applications, it is also necessary to predict diffuse and global irradiance. It is the purpose of this contribution to propose a complete and high-performance model to predict direct, diffuse and global irradiance. This goal is achieved by improving the algorithms that were used to obtain the earlier two-band CPCR2 model (Gueymard, 1989b), which has been validated by various studies (see, e.g., Battles et al., 2000; Gueymard, 1993a; Ineichen, 2006; Olmo et al., 2001). Despite these good results, modelling improvements are now deemed justified by the fact that CPCR2 has been developed in the early 1980s, a period after which the fields of atmospheric radiative transfer modelling and radiative

E-mail address: Chris@SolarConsultingServices.com
[1] ISES member.

0038-092X/$ - see front matter © 2007 Elsevier Ltd. All rights reserved.
doi:10.1016/j.solener.2007.04.008

measurements have made considerable progress. Four important scientific achievements of the 1980–2005 period can be specifically singled out for further discussion: (i) the high-resolution (e.g., line-by-line) absorption properties of many atmospheric gases have been obtained by spectrometry and are now described in large databases such as HITRAN (Rothman et al., 2005), to which many atmospheric radiative codes refer; (ii) better knowledge of the optical properties of aerosols and refined modelling of their scattering effects are now available; (iii) new experimental techniques and calibration procedures for the precise measurement of diffuse and global irradiance have emerged on the path of optimal measurement procedures (Michalsky et al., 1999), yielding significantly better accuracy under clear skies in particular (Michalsky et al., 2005), and therefore also better reference datasets for performance assessment studies; and (iv) specialized ancillary measurements describing the current atmospheric conditions are now carried out (from ground or space) more precisely, more frequently, and with a better spatial distribution than ever before, hence providing more complete and accurate inputs to the most detailed radiative models. All these factors do contribute to more efficient modelling and are appropriately used (directly or indirectly) in what follows. The goal here is to predict irradiances under cloudless conditions with accuracies comparable to that of the best radiometers, but without the need for spectral radiative models such as SMARTS (Gueymard, 2001) or SOLIS (Mueller et al., 2004), whose input data and file management requirements are substantially more challenging.

The present contribution is limited to the deterministic prediction of solar irradiance, illuminance and photosynthetically active radiation (PAR) under cloudless skies. Studies are underway to propose a cloud transmittance algorithm as well.

2. Modelling issues

As shown in previous studies (Gueymard, 1993a, 2003b,a) the performance of a broadband model under cloudless skies is determined in great part by that of the algorithm and input it uses to describe the aerosol transmittance, simply because aerosols are normally the major source of extinction under clear skies. A general finding common to these studies is that models that perform best are those whose aerosol algorithm is sufficiently detailed, and rely on spectral aerosol optical depth data. From the Bouguer–Beer–Lambert law, the spectral aerosol transmittance, $T_{a\lambda}$, can be obtained as

$$T_{a\lambda} = \exp(-m\tau_{a\lambda}) \tag{1}$$

where $\tau_{a\lambda}$ is the spectral aerosol optical depth (AOD) along a vertical atmospheric column and m is the relative slant pathlength (or "air mass"). Because $\tau_{a\lambda}$ is not constant over the spectrum, and the radiation impinging on the aerosol layer is already attenuated by the above atmospheric layers, the often-used extrapolation of Eq. (1) to the broadband domain

$$T_a = \exp(-m\tau_a) \tag{2}$$

(where T_a is the broadband aerosol transmittance and τ_a is the broadband AOD) cannot produce correct results. This fact led to the development of substantially more complicated – but also more accurate – transmittance expressions, as used in the MLWT2 or REST models (Gueymard, 2003a).

A related issue is that, until the late 1990s, there was no reliable, comprehensive, or readily available source of spectral AOD data covering the globe. This has changed dramatically with the development of various sunphotometric ground networks, such as AERONET (Holben et al., 1998). For even wider geographic coverage, it is also possible to use gridded AOD data from various satellite-borne sensors or from chemical transport models. Even though their current accuracy is still not comparable to that of ground-based sunphotometers, it is anticipated that major improvements in instrumentation, retrieval algorithms or aerosol transport modelling will provide a wealth of sufficiently accurate data in the coming years, as discussed further in Section 4.

3. Derivation of the REST2 model

Previous results from in-depth performance assessment studies (Battles et al., 2000; Gueymard, 1993a; Olmo et al., 2001) have shown that the CPCR2 two-band model (Gueymard, 1989b) was a top performer when compared to simpler broadband models. A recent and thorough study (Gueymard, 2003b,a) demonstrated that CPCR2 performed consistently well to predict direct normal irradiance (DNI), under both ideal and realistic conditions. However, two newly introduced models (Gueymard, 2003a) tended to perform as well or better than CPCR2 for that purpose. These new models, REST and MLWT2, are however limited to the prediction of DNI and are therefore not "all purpose" models, as mentioned earlier. In this contribution, a high-performance model is therefore developed to use the general features of CPCR2 (two-band structure for accuracy, modelling of direct, diffuse and global irradiance) and update its transmittance functions – which were based on now 25-year-old spectral information – using the same basis as in REST. Hence the REST2 acronym (Reference Evaluation of Solar Transmittance, 2 bands), a two-band version of the REST model but with more capabilities. A preliminary version of the model has been presented previously (Gueymard, 2004b). The present contribution describes some new features of the model, includes its latest algorithmic improvements, and proposes a benchmark dataset for the performance assessment of this or any other similar model.

The general structure of REST2 is almost identical to that of CPCR2, with a band separation at 0.7 μm. *Band 1* covers the UV and visible, from 0.29 to 0.70 μm. It is

characterized by strong absorption by ozone in the UV and strong scattering by molecules and aerosols over the whole band. *Band 2* covers the near-infrared, from 0.7 to 4 μm, and is characterized by strong absorption by water vapor, carbon dioxide and other gases, along with only limited scattering. This modelling approach has been used in a few other models of the literature and has been shown to have two interesting advantages: (i) it improves accuracy compared to regular single-band models (by essentially avoiding the limitations of Bouguer–Beer–Lambert's law mentioned above); and (ii) it simplifies the derivation of illuminance and photosynthetically active radiation, whose spectral ranges correspond almost perfectly to Band 1, as detailed in Section 3.3.

Using the latest extraterrestrial spectral energy distribution and latest solar constant value of 1366.1 W/m^2 (Gueymard, 2004a), the extra-atmospheric irradiances at the mean sun-earth distance are $E_{0n1} = 635.4$ W/m^2 (or 46.51%) and $E_{0n2} = 709.7$ W/m^2 (or 51.95%) in the two bands, respectively. To the difference of CPCR2, the parameterizations for direct and diffuse irradiance take into account the circumsolar radiation subtended in the typical 5.7°-total field-of-view of tracking devices (pyrheliometers or pyranometer shades).

3.1. Direct irradiance

The formalism is essentially the same as in CPCR2, except that additional provision is made for nitrogen dioxide absorption, as in REST. For each of the two-bands, i, the band direct normal irradiance, E_{bni}, is obtained from a product of individual transmittances:

$$E_{bni} = T_{Ri} T_{gi} T_{oi} T_{ni} T_{wi} T_{ai} E_{0ni} \tag{3}$$

where T_{Ri}, T_{gi}, T_{oi}, T_{ni}, T_{wi}, and T_{ai} are the band transmittances for Rayleigh scattering, uniformly mixed gases absorption, ozone absorption, nitrogen dioxide absorption, water vapor absorption and aerosol extinction, respectively.

These transmittances have been obtained accurately by fitting a large number of parametric runs of the SMARTS code (Gueymard, 2001, 2005b), version 2.9.5, to computationally efficient polynomial ratios. Only minimal errors are introduced by this parameterization, which in turn always guarantees good results because of the validated accuracy of the SMARTS absorption[2] and scattering algorithms in the first place (Gueymard, in press), and the model's independence from any empirical coefficient. The resulting equations are provided in Appendix 1.

Rather than a single air mass to characterize the solar rays' pathlength through the atmosphere, individual optical masses, m_R, m_o, m_w and m_a, are used for Rayleigh (molecular) scattering and uniformly mixed gases absorption, ozone absorption, water vapor absorption, and aerosol extinction, respectively. They are obtained from the sun's zenith angle, Z, with the same functions as in REST (Gueymard, 2003a). The molecular optical mass, m_R, is also called "relative air mass", and will be referred to simply as "air mass" in what follows.

The required atmospheric inputs to the model are: site pressure, p (hPa); ozone amount, u_o (atm-cm); total nitrogen dioxide amount, u_n, (atm-cm); precipitable water, w (cm), and Ångström turbidity coefficients, α_1, α_2, and β, where α_1 and α_2 are the respective values of α for each band. In realistic cases, α_1, α_2 and β can be derived from spectral irradiance measurements (conducive to AOD) from n discrete aerosol channels using a linearization of Ångström's law:

$$\ln \tau_{a\lambda} = \ln \beta_i - \alpha_i \ln \lambda \tag{4}$$

where λ is wavelength in μm. The coefficients $\ln \beta_i$ and $-\alpha_i$, respectively, represent the intercept and (negative) slope of the fitted straight line to the n data pairs ($\tau_{a\lambda}$, λ). This fit can be performed independently for wavelengths below and above 700 nm to obtain (α_1, β_1) and (α_2, β_2), respectively, with the constraints

$$\beta_1 = \beta 0.7^{\alpha 1 - \alpha 2}, \quad \beta_2 = \beta \tag{5}$$

In the case when such a detailed two-band analysis cannot be made, it can be assumed that $\alpha_1 = \alpha_2 = \alpha$. Typical values of α vary between about 0.5 and 2.5, depending on the source of aerosols and their size distribution. (The frequently quoted 1.3 value is only representative of rural or continental aerosols.)

The proposed parameterizations are valid at least for these wide input ranges $300 < p < 1100$ hPa; $0 < u_o < 0.6$ atm-cm; $0 < u_n < 0.03$ atm-cm; $0 < w < 10$ cm; $0 < \alpha_i < 2.5$; and $0 < \beta < 1.1$.

Aerosol extinction is carefully modelled. Its band-average optical depth uses the same formalism as in the original Ångström equation, but considers an effective wavelength for the whole band, λ_{ei}, as in CPCR2:

$$\tau_{ai} = \beta_i \lambda_{ei}^{-\alpha i} \tag{6}$$

where β_1 and β_2 are obtained from Eq. (5). Each band's aerosol transmittance is therefore

$$T_{ai} = \exp(-m_a \tau_{ai}) \tag{7a}$$

It has been found that λ_{ei} is essentially a function of $u_a = \ln(1 + m_a \beta_i)$ (Gueymard, 1989b). The revised functions used here to obtain λ_{ei} are described in Appendix 1.

Aerosol extinction is mostly caused by scattering, and by absorption for the remaining part. The aerosol scattering transmittance is expressed as

$$T_{asi} = \exp(-m_a \omega_i \tau_{ai}) \tag{7b}$$

where ω_i is the single-scattering albedo. Its value depends on the dominant type of aerosols, and typical values are listed in Table 1 of (Gueymard, 1989b). For general use, the typical values $\omega_1 = 0.92$ and $\omega_2 = 0.84$ are

[2] Recent spectroscopic data of absorption cross-sections are used in SMARTS.

recommended. Note that the REST2 aerosol transmittance can be calculated for very hazy conditions, covering for example the case of heavy smoke plumes and dust storms (during which β can reach or exceed 1.0), whereas the aerosol functions in CPCR2 were limited to $\beta < 0.5$.

The broadband DNI is simply obtained as the sum of the two-band components: $E_{bn} = E_{bn1} + E_{bn2}$.

3.2. Diffuse and global irradiance

Like for CPCR2, the formalism is here based on a two-layer scattering scheme. The top layer is assumed the source for all Rayleigh scattering, as well as for all ozone and mixed gas absorption. Similarly, the bottom layer is assumed the source for all aerosol scattering, as well as for aerosol, water vapor and nitrogen dioxide absorption. After scattering has occurred in the top layer, the downwelling diffuse irradiance is assumed to behave as direct irradiance at an effective air mass, $m' = 1.66$. This is the air mass value that is used in calculating the transmittances (indicated with a prime in what follows) dealing with absorption in the bottom layer.

The incident diffuse irradiance on a perfectly absorbing ground (i.e., with zero albedo) is defined as

$$E_{dpi} = T_{oi}T_{gi}T'_{ni}T'_{wi}\left[B_{Ri}(1-T_{Ri})T_{ai}^{0.25} + B_a F_i T_{Ri}\left(1-T_{asi}^{0.25}\right)\right]E_{0i} \quad (8)$$

where

$$E_{0i} = E_{0ni}\cos Z \quad (9)$$

Function F_i is a correction factor introduced to compensate for multiple scattering effects and other shortcomings in the simple transmittance approach used here. B_{R1} and B_{R2} are the forward scattering fractions for Rayleigh extinction. In the absence of multiple scattering, they would be exactly 0.5 because molecules scatter equally in the forward and backward directions. Multiple scattering is negligible in Band 2 (so that $B_{R2} = 0.5$), but not in Band 1. Using a simple spectral model to describe this effect (Skartveit and Olseth, 1988), B_{R1} is obtained after spectral integration and parameterization as

$$B_{R1} = 0.5(0.89013 - 0.0049558 m_R + 0.000045721 m_R^2) \quad (10)$$

The aerosol forward scatterance factor, B_a, is the same as in CPCR2:

$$B_a = 1 - \exp(-0.6931 - 1.8326\cos Z) \quad (11)$$

The beam, diffuse and global broadband irradiances incident on a horizontal and ideally black surface are finally $E_b = E_{bn}\cos Z$, $E_{dp} = E_{dp1} + E_{dp2}$, and $E_{gp} = E_b + E_{dp}$, respectively.

Under normal conditions, a backscattered contribution must be added because of the interaction between the reflecting earth surface and the scattering layers of the atmosphere. This contribution is usually small (e.g., <10% of E_{gp}) but may become far more significant over snowy regions. The ground albedo to consider here, ρ_g, refers to an average over a large zone of 5–50 km radius around the site under scrutiny, per the discussion in (Gueymard, 1993b). For each band, the sky albedo, ρ_{si}, is obtained as a function of α_i and β_i, and the backscattered diffuse component, E_{ddi}, is derived by considering multiple reflections between the ground and the atmosphere

$$E_{ddi} = \rho_{gi}\rho_{si}(E_{bi} + E_{dpi})/(1 - \rho_{gi}\rho_{si}) \quad (12)$$

where $E_{bi} = E_{bni}\cos Z$. Finally, the total diffuse irradiance in each band is $E_{di} = E_{dpi} + E_{ddi}$, so that the broadband diffuse irradiance is obtained as $E_d = E_{d1} + E_{d2}$ and the broadband global irradiance as $E_g = E_b + E_d$.

The effect on DNI of air mass for reference conditions ($p = 1013.25$ hPa, $u_o = 0.35$ atm-cm, $u_n = 0.0002$ atm-cm, $w = 1.5$ cm), and variable turbidity, is shown in Fig. 1. Similarly, the effect on direct, diffuse and global irradiance of progressively varying β is shown in Figs. 2–4 for three air masses ($m_R = 1$, 2 and 5; i.e., $Z = 0°$, 60° and 79°, respectively) and three wavelength exponents ($\alpha = 0$, 1.3 and 2.5, with $\alpha_1 = \alpha_2 = \alpha$). Fig. 3 shows the non-trivial effect of β on diffuse irradiance. The latter increases with β only if β is below some threshold (whose exact value is an intricate function of α, β and Z), at which points it peaks and then decreases when β continues to increase. This reversal of behavior is attributed to the concomitant strengthening of multiple scattering effects. It also interferes with the normal compensation between direct and diffuse irradiance that holds under low turbidity conditions and normally results in only modest decrease in global irradiance when turbidity increases. As a result, the effect of turbidity on global irradiance is potentially larger than generally admitted.

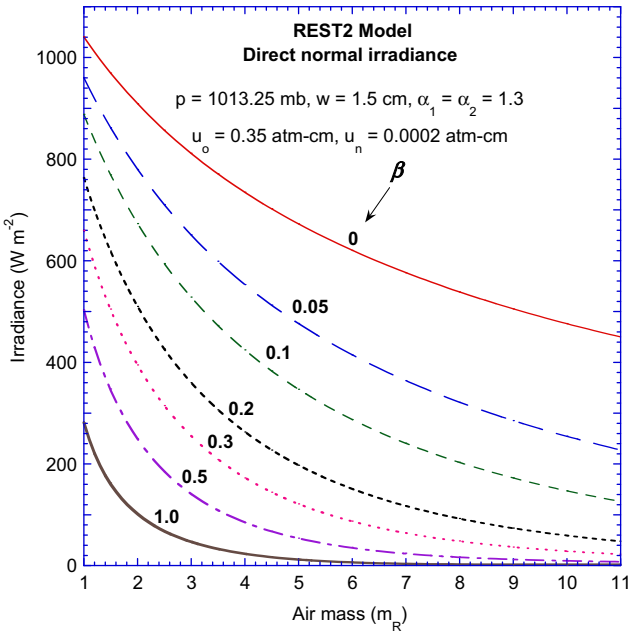

Fig. 1. Direct normal irradiance predicted by REST2 as a function of air mass for fixed reference atmospheric conditions except variable turbidity.

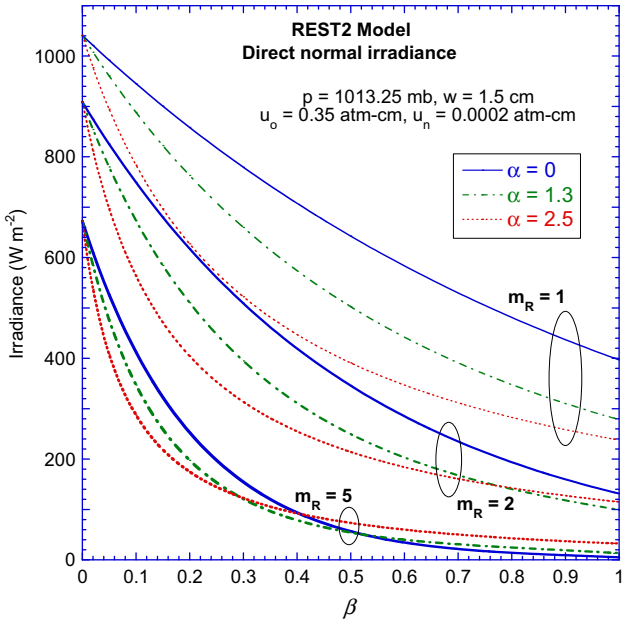

Fig. 2. Direct normal irradiance predicted by REST2 as a function of turbidity for three air mass values (1, 2 and 5) and otherwise fixed reference atmospheric conditions.

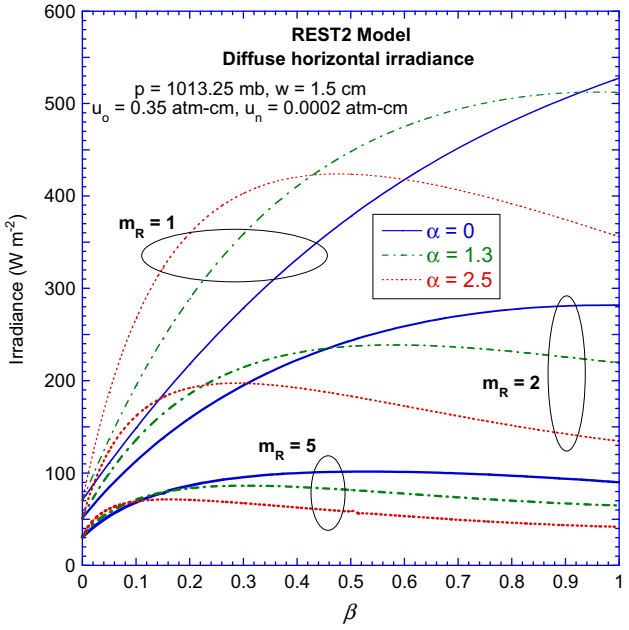

Fig. 3. Diffuse horizontal irradiance predicted by REST2 as a function of turbidity for three air mass values (1, 2 and 5) and otherwise fixed reference atmospheric conditions.

3.3. Illuminance and photosynthetically active radiation

As was shown before (Gueymard, 1989b), an interesting advantage of a two-band irradiance model is that it can also be easily used to derive photosynthetically active radiation (PAR) and illuminance from the Band 1 irradiance calculations, because all these quantities share a similar

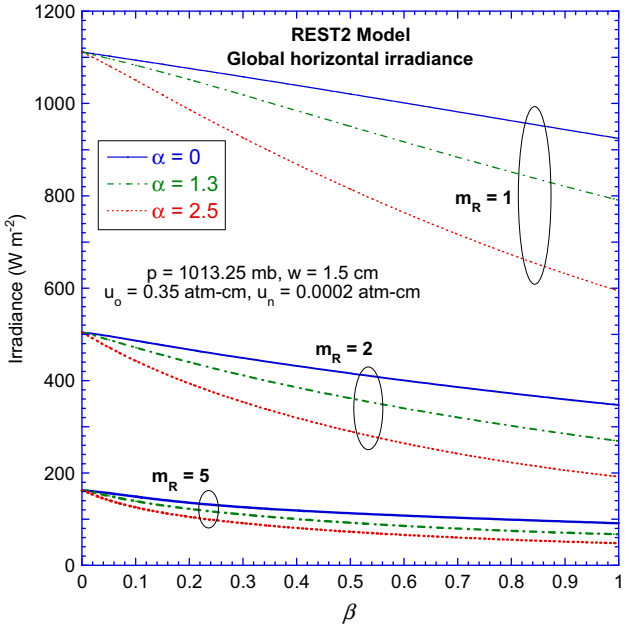

Fig. 4. Global horizontal irradiance predicted by REST2 as a function of turbidity for three air mass values (1, 2 and 5) and otherwise fixed reference atmospheric conditions.

wavelength range. Illuminance and PAR can be obtained directly as

$$L_j = E_{j1} K_j \tag{13}$$

and

$$P_j = E_{j1} M_j \tag{14}$$

where L_j is illuminance (lx), K_j is the Band 1 luminous efficacy (lm/W), P_j is PAR irradiance (W/m^2), M_j is the Band 1 to PAR conversion factor (unitless), and j stands for either b (beam) or g (global), depending on which component is dealt with.

Simple parameterizations for K_j and M_j were initially presented for use with CPCR2 (Gueymard, 1989b). Their simplicity was not conducive to top performance, as was revealed in later studies (Alados-Arboledas et al., 2000; Gueymard, 2005a). A more detailed formulation is presented in what follows, obtained this time by precisely parameterizing the SMARTS results.

Illuminance is obtained spectrally from

$$L_j = K_m \int_{\lambda_0}^{\lambda_1} v_\lambda E_{j\lambda} \, d\lambda \tag{15}$$

where L_j stands for either L_b, the beam horizontal illuminance, or L_g, the global horizontal illuminance. Similarly, $E_{j\lambda}$ stands for either $E_{b\lambda}$, the beam horizontal spectral irradiance, or $E_{g\lambda}$, the global horizontal spectral irradiance at wavelength λ. K_m is the maximum luminous efficacy, 683 lm/W, and v_λ is the "V_M-lambda" CIE curve describing the eye's relative response for photopic vision, according to the 1988 curve. [See the relevant references and a discussion about the difference between the 1931 and

1988 photopic curves in (Darula et al., 2005).] The numerical integration is performed between $\lambda_0 = 0.38$ μm and $\lambda_1 = 0.78$ μm and provides results in lx.

The ratios L_b/E_{b1} and L_g/E_{g1} – where $E_{b1} = E_{bn1}\cos Z$ and $E_{g1} = E_{b1} + E_{d1}$ are obtained with the method described above – have been calculated for various combinations of input values. As could be expected, the main variables affecting these ratios are found to be air mass and turbidity. The proposed parameterization is

$$K_b = (r_0 + r_1\beta_e + r_2\beta_e^2)/(1 + r_3\beta_e^2) \quad (16)$$

$$K_g = (s_0 + s_1\beta_e + s_2\beta_e^2)/(1 + s_3\beta_e) \quad (17)$$

where all coefficients r_i and s_i (see Appendix 2) depend on m_R, and where the effective turbidity coefficient, β_e, is obtained from the previously defined β_1 and λ_{e1} as

$$\beta_e = \beta_1 \lambda_{e1}^{1.3-\alpha 1} \quad (18)$$

The cloudless diffuse illuminance, L_d, is simply obtained as the difference between L_g and L_b. Figs. 5–7, similarly to Figs. 2–4, demonstrate the strong effect of turbidity and air mass on all the components of illuminance. Interestingly, this turbidity effect is even more pronounced on illuminance than on irradiance. The REST2 illuminance model can advantageously replace indirect determinations of illuminance from broadband irradiance, which are usually based on luminous efficacy functions (see, e.g., Gueymard, 1995; Lopez and Gueymard, 2007 and references therein).

PAR irradiance is defined spectrally as

$$P_j = \int_{\lambda_2}^{\lambda_3} E_{j\lambda}\, d\lambda \quad (19)$$

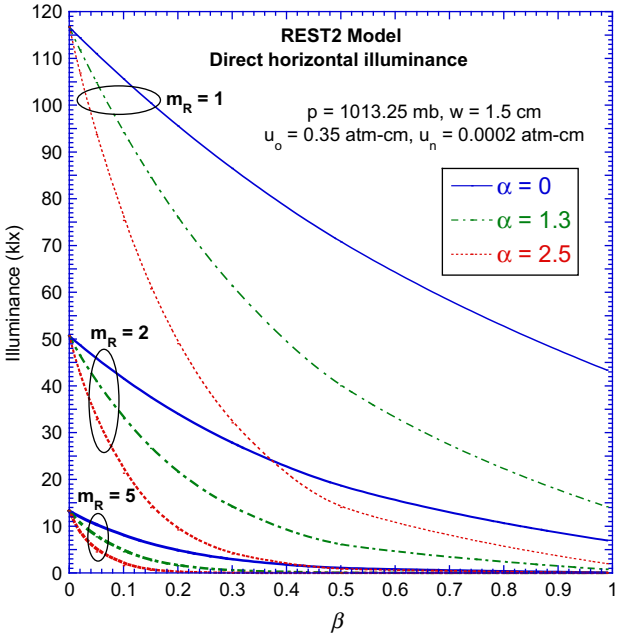

Fig. 5. Direct horizontal illuminance predicted by REST2 as a function of turbidity for three air mass values (1, 2 and 5) and otherwise fixed reference atmospheric conditions.

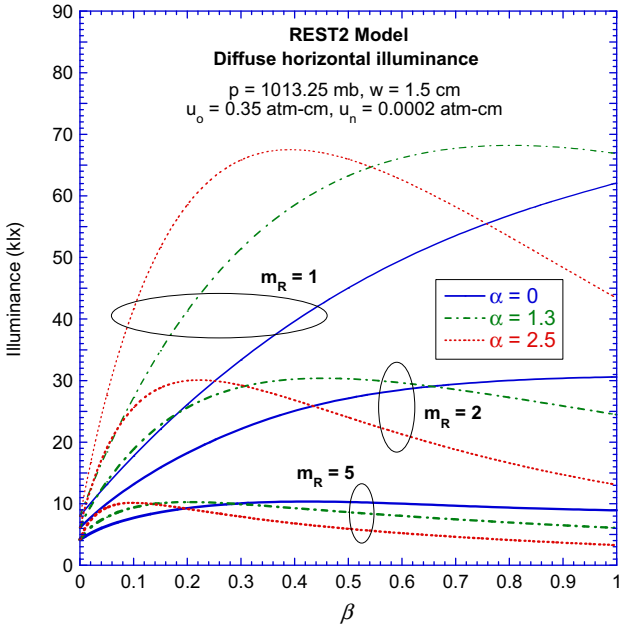

Fig. 6. Diffuse horizontal illuminance predicted by REST2 as a function of turbidity for three air mass values (1, 2 and 5) and otherwise fixed reference atmospheric conditions.

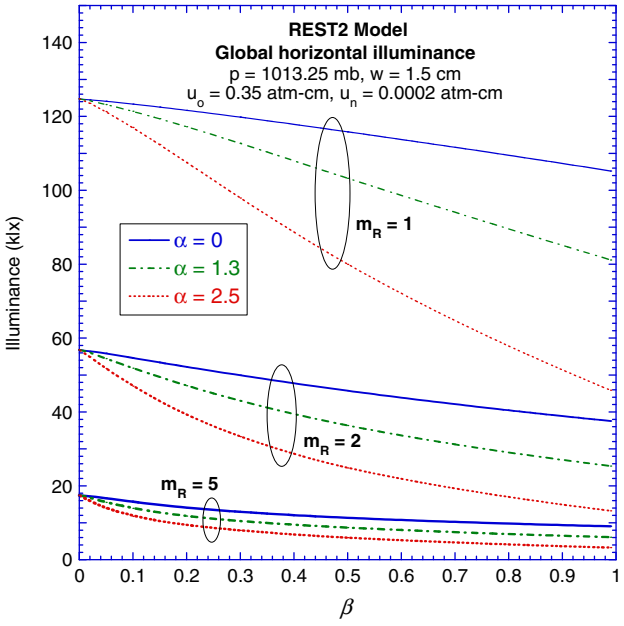

Fig. 7. Global horizontal illuminance predicted by REST2 as a function of turbidity for three air mass values (1, 2 and 5) and otherwise fixed reference atmospheric conditions.

where $\lambda_2 = 0.4$ μm and $\lambda_3 = 0.7$ μm. The ratios $M_j = P_j/E_{j1}$ are obtained in a similar manner as for illuminance and are parameterized as

$$M_b = (t_0 + t_1\beta_e + t_2\beta_e^2)/(1 + t_3\beta_e^2) \quad (20)$$

$$M_g = (v_0 + v_1\beta_e + v_2\beta_e^2)/(1 + v_3\beta_e^2) \quad (21)$$

where all coefficients t_i and v_i (see Appendix 2) again depend on m_R. The diffuse PAR irradiance is simply obtained by difference, $P_d = P_g - P_b$.

Plots of the effect of air mass and turbidity on PAR irradiance appear in Figs. 8–10. In addition to confirming the large effect of turbidity on all the PAR irradiance components (similar to the effect it has on illuminance), these plots also show that PAR often consists primarily of diffuse radiation. Various studies (see, e.g., Gu et al., 2002; Roderick et al., 2001 and references therein) have demonstrated the positive effect of turbidity increases on the productivity of plants. A key factor to plant growth is therefore how the diffuse/global radiation ratio, P_d/P_g, is related to turbidity. In this respect, the variation of P_d/P_g as affected by the two turbidity coefficients α and β, has been calculated with REST2, SMARTS and an older model (Gueymard, 1989a) that calculates PAR directly (i.e., without preliminary knowledge of any broadband irradiance). These results confirm that P_d/P_g increases rapidly with β, α or m_R. An example of such results is illustrated in Fig. 11 for the specific case of $Z = 60°$ ($m_R = 2$). The steep gradient of P_d/P_g vs. β appears very clearly, but the role of α is significant too. The three cases chosen are typical of aerosols of different origins. The value of α is inversely related to the aerosol particles' average size. The larger aerosols (with typically $\alpha = 0.5$) can be of maritime, desert or volcanic origin. The average aerosols ($\alpha = 1.3$) are normally of rural or continental origin. The smallest aerosols ($\alpha = 2.5$) are found in either pristine/remote or polluted/urban environments. Interestingly, the predictions of the three models are in good agreement, despite their widely different algorithms. As could be expected, the older PAR model deviates more from SMARTS than REST2 because of its simpler algorithm, based on now outdated extinction data. Furthermore, only REST2 and SMARTS take the effect of NO_2 into consideration, which might be significant in polluted environments.

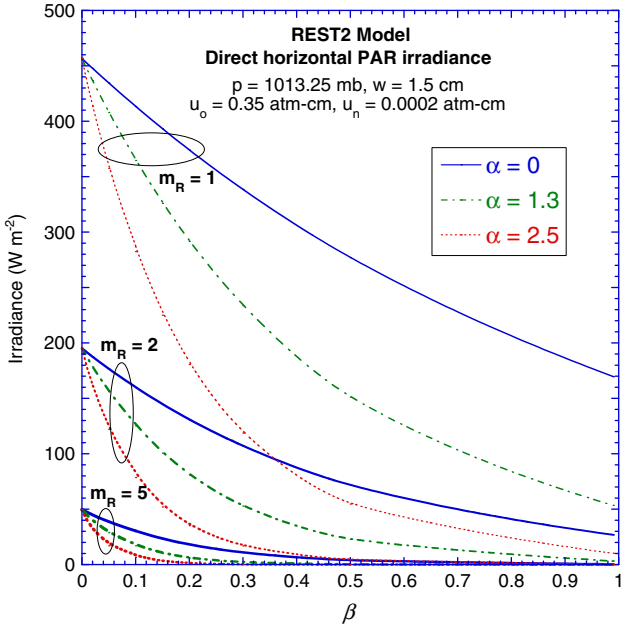

Fig. 8. Direct horizontal PAR irradiance predicted by REST2 as a function of turbidity for three air mass values (1, 2 and 5) and otherwise fixed reference atmospheric conditions.

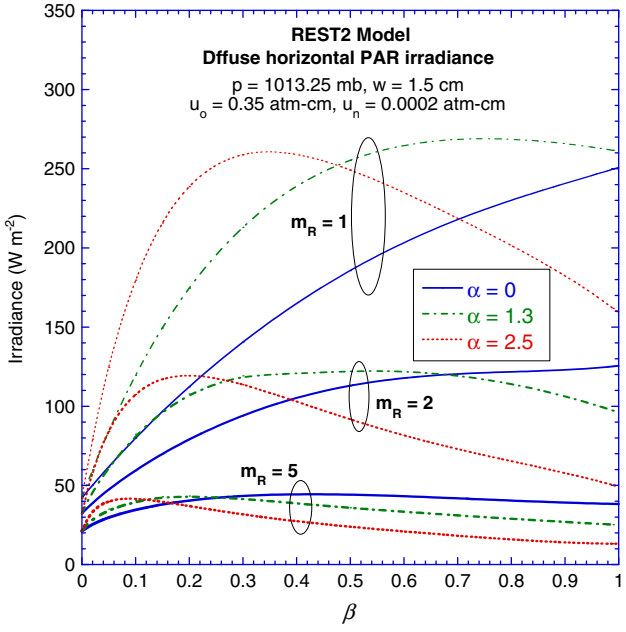

Fig. 9. Diffuse horizontal PAR irradiance predicted by REST2 as a function of turbidity for three air mass values (1, 2 and 5) and otherwise fixed reference atmospheric conditions.

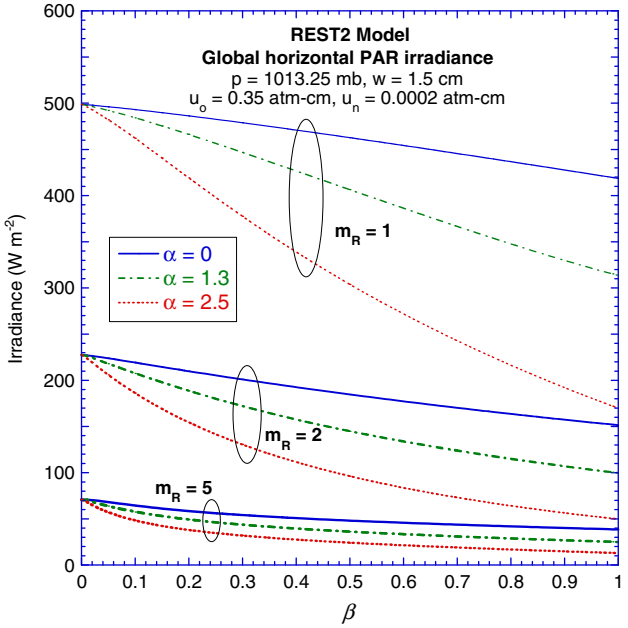

Fig. 10. Global horizontal PAR irradiance predicted by REST2 as a function of turbidity for three air mass values (1, 2 and 5) and otherwise fixed reference atmospheric conditions.

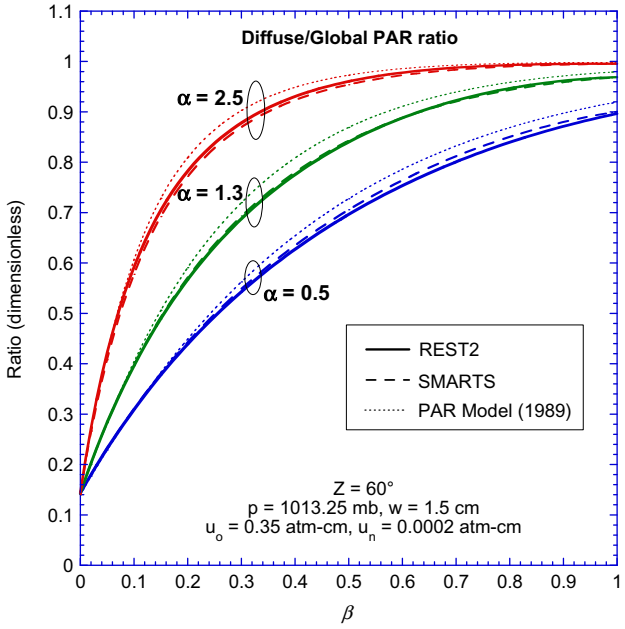

Fig. 11. Diffuse-to-global horizontal PAR irradiance ratio predicted by REST2, SMARTS and the PAR model of (Gueymard, 1989) as a function of turbidity for three values of Ångström's wavelength exponent α (0.5, 1.3, and 2.5), a fixed air mass of 2, and otherwise fixed reference atmospheric conditions.

4. Turbidity data availability

As discussed above, the prediction of irradiance, illuminance or PAR with REST2 depends heavily on the turbidity coefficients α_i and β, rather than on a single one, such as τ_a or the Linke turbidity factor, T_L, as in many older models. Despite the added complexity, relying on more than one turbidity variable has considerable advantages: first, this eliminates the problems associated with the derivation and limited availability of τ_a or T_L (which cannot be directly measured, and are therefore dependent in both magnitude and accuracy on a radiation model); and, second, this benefits from the current rapid developments in the measurement of AOD. These developments are largely driven by the need for accurate optical depth data to obtain ground truth for satellite remote-sensing, or to evaluate the aerosol radiative forcing in climate change studies. In particular, the spectral (rather than broadband) AOD is necessary for these studies, hence the lost interest in τ_a or T_L within the climatology community.

There are currently three important sources of AOD data: ground-based sunphotometric networks, chemical transport models, and satellite-based spectroradiometers. The latter source is most likely the way of the future because of the world coverage it permits, with relatively fine spatial and temporal resolution. Moreover, quasi real-time analysis of satellite images already allows the rapid detection of dust storm events or smoke plumes caused by heavy pollution or biomass fires, which in turn all induce high-turbidity, low-visibility conditions on their path, and hence depleted irradiance episodes (Gueymard et al., 2000). The difficulty here, however, is that the AOD retrieval from space is still not very accurate, especially with regard to clean environments, because the aerosol signal is relatively weak compared to that of clouds or other highly reflective surfaces (e.g., light sand or snow). Progress in instrumentation and algorithms is nevertheless very fast, so that the accuracy of spaceborne AOD data is constantly improving.

An essential component in this progress is the use of ground truth data to calibrate or assess the performance of retrieval algorithms or transport models. Such ground truth is obtained with multiwavelength radiometers from specialized networks, the largest of which is AERONET (http://aeronet.gsfc.nasa.gov), with hundreds of sites worldwide.

Typically, both AOD and precipitable water (evaluated from a dedicated channel in the 940-nm spectral band) can be obtained from these spectral measurements. For each single multiwavelength data point, the Ångström coefficients α and β can be simply derived by linearly fitting the measured AODs using Eq. (4). Ongoing work is aimed at mapping the monthly average α and β at the continental scale (Gueymard and George, 2005).

5. Model's performance assessment

It is now known (Gueymard, 2003b) that the accuracy of the best broadband models predicting DNI is comparable to that of irradiance measurements in networks. Therefore, the performance of a good model needs to be assessed against measurements of the highest-quality (i.e., research-grade radiometric data). The latter can only be obtained if three key ingredients are present: first-class instrumentation, sophisticated calibration/correction procedures, and extensive quality control.

In recent years, the quality of radiation measurements became a source of concern because of the need for lowered measurement uncertainties in climate change studies, which led to the discovery that conventional instrumental techniques had significant errors. Systematic errors were found in diffuse and global irradiance measurements, particularly under clear skies, therefore increasing the experimental uncertainty. As a result, better calibration techniques have been developed, as well as empirical corrections for the daytime offset (caused by thermal imbalance) and cosine error of pyranometers, and better quality-control procedures (see, e.g., Cess et al., 2000; Michalsky et al., 1999; Myers et al., 2002; Philipona, 2002). Recent studies (Michalsky et al., 2005, 2007) have helped define reference diffuse measurements, using pyranometers with specific characteristics and forced ventilation (to minimize thermal imbalance effects), and a tracking shade (to avoid the uncertainties inherent to the use of a shade ring). Nevertheless, the most far-reaching outcome of these studies is certainly that state-of-the-art instrumentation for global radiation is now defined as a combination of a pyrheliometer (for direct radiation) and a shaded pyranometer (for

diffuse radiation, as described just above). This means that global irradiance is now best *calculated* as the sum of its direct and diffuse horizontal components, rather than directly measured as usual with an unshaded pyranometer. Experimental sites from the Baseline Surface radiation Network (BSRN, http://bsrn.ethz.ch/) follow all these rules, and therefore offer the highest-quality datasets to test irradiance predictions.

In what follows, a short performance assessment study is offered, using a set of 30 individual measurements obtained at the Southern Great Plain (SGP) site of Billings, Oklahoma, USA during the Aerosol Intensive Observation Period (AIOP) of May 2003, which was conducted under the auspices of the Atmospheric Radiation Measurement program (ARM, http://www.arm.gov). This experimental site is also a member of the BSRN network. Instrumentation used during this AIOP included both an active cavity radiometer and a pyrheliometer for direct radiation, and two pyranometers (one black-and-white Eppley 8-48, insensitive to thermal offset, and one offset-corrected Kipp & Zonen CM22) for diffuse radiation. More details of the experiment and measurements are given elsewhere (Michalsky et al., 2006). It is important to note that the latter contribution (i) involved many ancillary measurements of atmospheric conditions with co-located instruments, particularly related to aerosols, and therefore allowed a real radiative closure experiment; and (ii) demonstrated that, on average, *spectral* radiation models are able to predict direct and diffuse broadband irradiance within the radiometers' experimental error, therefore achieving closure. It is argued that this dataset constitutes the first modern benchmark to test spectral or broadband irradiance models, hence the special treatment it receives in what follows, and the fully disclosed details, which are provided for future reference.

It is emphasized that a radiative closure experiment is necessary to test the performance of a model, with accurate independent and coincident measurement of all the atmospheric inputs to the model, in order to avoid any inadvertent error that would be caused by error propagation from inaccurate inputs. This is particularly important in the case of the aerosol optical properties, because they essentially control the performance of radiation models under clear skies. Considerable degradation of the apparent performance of a model usually results from the use of time-averaged or spatially extrapolated input data, for instance, as has been experimentally verified elsewhere (Battles et al., 2000; Ineichen, 2006; Olmo et al., 2001).

The original dataset that was sent to the participants of the aforementioned closure experiment contained spectral measurements of AOD and ground albedo. For the present broadband application, the Ångström coefficients α_1, α_2 and β were obtained from spectral AOD using the procedure explained above (Eq. (4)). The broadband ground albedo for each individual case was evaluated by spectrally integrating the spectral ground albedo (measured from a tower), $\rho_{g\lambda}$, using

$$\rho_g = \int_{0.3}^{3.0} \rho_{g\lambda} E_{gp\lambda}\, d\lambda \Big/ \int_{0.3}^{3.0} E_{gp\lambda}\, d\lambda \tag{22}$$

where $E_{gp\lambda}$ is the global irradiance incident on a black ground, as calculated by SMARTS. Note that the 30 data points are associated with relatively large variations in ground albedo (from 0.107 to 0.201, average 0.150), considering the short 26-day experiment period. Closer inspection shows that this change in albedo is well correlated with change in zenith angle. This effect is caused by the non-isotropic nature of the ground reflection process (see, e.g., Gueymard, 1987). For comparative purposes, the average ground albedo over a 7×7 km^2 area centered on the measurement site was 0.156 for the 16-day period of 9–24 May 2003, as retrieved by the MODIS-Terra spaceborne instrument. This is in excellent agreement with the average ground albedo obtained here from tower measurements, owing to the homogeneous land use of the area.

The aerosol single-scattering albedo was originally obtained at 550 nm from in situ measurements of air samples. It is assumed here that this single spectral value, ω_0, can be used to represent both ω_1 and ω_2. For the total columnar NO_2 amount, a constant abundance of 0.3 matm-cm is assumed in all cases, based on remote-sensing data from the SCIAMACHY instrument (http://www.iup.unibremen.de/doas/scia_data_browser.htm).

Table 1 summarizes all the input data necessary to use REST2 or CPCR2. This table also provides the usual performance statistics (standard deviation and percent Mean Bias Difference (MBD) and Root Mean Square Difference (RMSD) with reference to the measured data) of REST2 for the whole dataset, compared to those obtained with CPCR2. By comparison with previous results (Michalsky et al., 2006), it is found that REST2's agreement with the measured data is nearly as good as that of SMARTS, suggesting that the broadband parameterization is very effective. Results in Table 1 also show that the prediction of diffuse radiation is noticeably improved compared to CPCR2, and that REST2 can effectively predict irradiance within the experimental uncertainty, provided of course that accurate input data are used.

It is also desirable to test the performance of REST2's predictions of illuminance and PAR in a similar way as with irradiance. Unfortunately, no illuminance or PAR sensor is available at the ARM-SGP site considered here. Nevertheless, it is possible to obtain these quantities indirectly by spectral integration of global, diffuse and direct irradiance spectra obtained with a co-located Rotating Shadowband Spectroradiometer (RSS). This sophisticated solid-state instrument uses an alternating shadowband to record global and diffuse irradiance spectra nearly simultaneously. The direct spectrum is obtained by difference. The effective spectral range of the instrument is 360–1070 nm, hence perfectly covering the wavebands under scrutiny here. The instrument's calibration is regularly performed (individually for each of the 1024 pixels), and its cosine error is compensated for. This results in a low experimental

Table 1
Benchmark dataset for the validation of radiation models, and irradiance results (in W/m^2) from the REST2 and CPCR2 models

Case #	Day[1]	CST[2]	Z[3]	p[4]	w[5]	u_o[6]	β[7]	α_1[8]	α_2[9]	ω_0[10]	ρ_g[11]	Measured irradiance–			REST2 predicted———-			CPCR2 predicted———-		
												DNI[12]	Diffuse	Global	DNI	Diffuse	Global	DNI	Diffuse	Global
–	5	0645	76.743	965.6	1.27	0.336	0.0417	0.0967	0.3931	0.888	0.185	604	51	190	600.2	51.2	188.7	628.7	50.3	194.4
2	5	0800	61.805	966.3	1.34	0.336	0.0446	0.0902	0.4035	0.930	0.169	**827**	70	461	804.5	75.6	455.6	820.9	76.3	463.9
3	5	0910	47.853	966.6	1.30	0.336	0.0337	0.6992	0.5190	0.930	0.154	**913**	78	691	906	80.9	689	906.7	86.7	695.3
4	5	1200	21.159	966.1	1.35	0.336	0.0410	0.6256	0.6865	0.918	0.130	**968**	95	998	964.8	96.7	996.5	962.1	102.4	999.6
5	5	1600	51.103	963.9	1.51	0.336	0.0527	0.5112	0.4483	0.949	0.156	859	90	629	856.6	93.2	631.2	860.5	98.5	639.0
6	5	1800	75.033	963.4	1.92	0.336	0.0621	0.3703	0.4246	0.927	0.176	571	64	211	565.4	64	210	587.6	64.3	216.0
7	6	1730	68.945	970.3	1.72	0.350	0.0567	1.3262	1.1925	0.929	0.185	643	83	314	648.2	83	315.9	651.1	87.6	321.6
8	6	1815	77.831	970.8	1.71	0.350	0.0548	1.3521	1.2240	0.918	0.178	474	58	158	480	58.6	159.7	489.8	59.7	162.9
9	7	0730	67.475	976.5	1.97	0.337	0.0535	1.3189	1.3678	0.925	0.178	669	82	338	663.8	84.7	338.9	674.4	88.3	346.5
10	7	0930	43.592	976.3	1.98	0.337	0.0414	1.1662	1.2760	0.853	0.152	**882**	96	735	873.9	95.1	728.2	878.2	99.8	736.0
11	9	0930	43.254	969.6	0.95	0.318	0.1624	0.7615	0.6597	0.950	0.152	757	184	735	756.8	187.2	738.5	743.3	205.7	747.2
12	9	1130	22.899	969.6	1.13	0.318	0.1930	0.7466	0.5710	0.935	0.132	798	220	955	797.5	221.9	956.4	777.9	249.8	966.5
13	9	1230	19.227	969.2	1.43	0.318	0.1754	0.7351	0.5381	0.944	0.129	816	205	975	816.2	210.1	980.7	798.2	237.7	991.4
14	10	0700	72.958	963.3	1.58	0.301	0.2664	1.0054	0.8925	0.952	0.184	263	128	205	262.6	123.6	200.5	258.2	139.9	215.5
15	11	0700	72.808	982.3	1.04	0.312	0.0348	0.9330	1.1488	0.972	0.181	681	60	261	677.6	62.4	262.6	695.9	63.4	269.0
16	11	0920	44.896	984.0	1.13	0.312	0.0364	1.4867	0.5789	0.971	0.149	910	87	732	907.7	91.8	734.9	888.1	109.8	739.1
17	11	1230	18.706	983.4	1.11	0.312	0.0347	1.3951	0.6249	0.944	0.130	971	91	1011	974.5	97.3	1020.2	956.5	114.9	1020.9
18	11	1500	38.540	982.2	1.14	0.312	0.0360	1.1853	0.5770	0.957	0.141	936	84	816	933.7	91.6	822.1	921.7	104.9	826.0
19	12	0730	66.712	985.7	1.40	0.323	0.0375	1.5278	0.5941	0.883	0.201	750	67	364	742.9	70.9	364.4	726.5	79.7	366.8
20	12	0950	38.921	985.4	1.54	0.323	0.0367	1.0991	1.2164	0.934	0.144	909	95	802	910.3	95.9	804.2	911.3	101.8	810.9
21	20	1400	26.299	990.6	2.26	0.294	0.0747	1.4364	1.3413	0.930	0.110	854	148	914	854.7	144.7	910.9	846.2	162.7	921.2
22	22	0800	59.579	985.3	2.43	0.309	0.0715	1.1597	1.4796	0.939	0.157	694	114	465	694.6	111	462.7	713.3	114.3	475.4
23	27	1300	16.876	986.4	1.35	0.334	0.1053	1.2753	1.5693	0.943	0.110	844	185	993	844.1	186.8	994.7	841.4	198.3	1003.4
24	27	1600	48.328	984.8	1.43	0.334	0.1093	0.9638	1.5101	0.954	0.136	732	160	647	738.3	158.5	649.5	755.4	159.8	662.2
25	28	0730	65.110	984.5	2.99	0.320	0.0738	1.4045	1.6696	0.930	0.157	**601**	106	359	603.3	104	357.9	625.0	108.1	371.1
26	28	1800	72.058	979.7	2.71	0.320	0.0633	1.2771	1.6709	0.951	0.161	534	81	246	537	81.2	246.6	568.1	82.5	257.5
27	29	0830	53.082	979.0	2.80	0.291	0.0573	1.1976	1.3027	0.938	0.137	**774**	105	570	769.8	104.8	567.2	781.7	111.7	581.1
28	29	1230	14.978	976.4	2.83	0.291	0.0556	1.0659	1.1893	0.946	0.107	**903**	117	989	897.6	119.3	986.5	901.8	129.1	1000.3
29	30	1130	19.363	967.9	3.48	0.293	0.0745	1.2408	1.1476	0.922	0.111	865	134	950	854.1	136.8	942.7	853.9	153.6	959.2
30	30	1445	33.208	967.7	3.16	0.293	0.0617	1.3671	1.3334	0.939	0.121	844	121	827	840.2	125.6	828.5	842.5	139.4	844.2
Min			14.976	963.3	0.95	0.291	0.0337	0.0902	0.3931	0.853	0.107	263	51	158	262.6	51.2	159.7	258.2	50.3	162.9
Max			77.840	990.6	3.48	0.350	0.2664	1.5278	1.6709	0.972	0.201	971	220	1011	974.5	221.9	1020.2	962.1	249.8	1020.9
Mean			47.979	975.4	1.80	0.321	0.0748	1.0273	0.9850	0.933	0.150	761.5	108.6	618.0	759.2	110.3	618.2	762.2	119.4	626.8
Std. Dev.			21.107	8.6	0.71	0.017	0.0552	0.3951	0.4286	0.025	0.026	163.4	44.5	295.4	161.9	44.4	296.0	155.3	50.7	296.4
MBD (%)															−0.3	1.5	0.0	0.1	9.9	1.4
RMSD (%)															0.8	3.0	0.6	2.0	13.0	1.6

[1] Day of May 2003.
[2] Central Standard Time (Universal Time – 6 h).
[3] Sun's zenith angle (°).
[4] Site pressure (hPa or mb).
[5] Precipitable water (cm).
[6] Ozone amount (atm-cm).
[7] Ångström's turbidity coefficient (i.e., AOD at 1 μm).
[8] Ångström's wavelength exponent for Band 1 (extrapolated from measurements between 0.415 and 0.673 μm).
[9] Ångström's wavelength exponent for Band 2 (extrapolated from measurements between 0.673 and 0.870 μm).
[10] Aerosol single-scattering albedo.
[11] Ground albedo.
[12] Bold numbers indicate measurements with active-cavity radiometer and minimal uncertainty.

uncertainty, less than 5% overall. Unfortunately, such experimental spectra were available only for 13 of the 30 points constituting the benchmark database described in Table 1. The experimental illuminance and PAR are obtained from these spectra through Eqs. (15) and (19). It is argued that such an indirect determination of illuminance and PAR is actually of equal or better accuracy compared to what would be obtained directly with dedicated sensors, because of their use of imperfect filters. Therefore, the small 13-point dataset used here is also proposed as a

Table 2
Benchmark dataset for the validation of illuminance models, and results from the REST2 and CPCR2 models for direct, diffuse and global illuminance (in klx) on a horizontal surface

Case #	Day[a]	CST[b]	Measured illuminance			REST2 predicted			CPCR2 predicted		
			Direct	Diffuse	Global	Direct	Diffuse	Global	Direct	Diffuse	Global
15	11	0700	21.2	7.7	28.8	20.2	8.1	28.3	20.7	9.2	29.9
16	11	0920	73.1	10.8	83.9	70.5	11.4	81.9	67.7	15.9	83.5
18	11	1500	105.1	11.4	116.5	101.5	11.8	113.3	99.5	15.6	115.2
19	12	0730	33.1	8.6	41.7	31.3	9.2	40.5	28.8	12.2	41.0
20	12	0950	81.7	11.9	93.5	78.4	12.1	90.5	79.0	13.7	92.6
21	20	1400	87.5	20.8	108.2	84.0	19.7	103.7	81.5	24.3	105.8
22	22	0800	37.9	16.0	53.9	37.5	15.3	52.7	37.8	17.0	54.8
23	27	1300	86.7	27.4	114.2	84.4	25.8	110.2	84.0	29.1	113.1
25	28	0730	50.4	23.4	73.8	25.8	14.9	40.7	25.7	16.9	42.6
26	28	1800	16.6	11.8	28.5	15.9	11.5	27.4	16.5	12.9	29.4
27	29	0830	53.7	14.3	68.0	51.7	14.0	65.7	51.4	16.3	67.7
28	29	1230	102.9	15.6	118.5	98.6	15.3	113.9	99.1	17.4	116.5
Min			16.6	7.7	28.5	15.9	8.1	27.4	16.5	9.2	29.4
Max			105.1	27.4	118.5	101.5	25.8	113.9	99.5	29.1	116.5
Mean			60.5	14.3	74.8	58.3	14.1	72.4	57.6	16.7	74.3
Std. Dev.			32.7	5.5	35.3	31.5	4.8	33.9	31.1	5.3	34.2
MBD (%)						−3.6	−2.4	−0.5	−4.7	16.8	−0.6
RMSD (%)						4.2	2.5	0.5	5.9	19.0	1.6

See Table 1 for atmospheric data in each case.
[a] Day of May 2003.
[b] Central Standard Time (Universal Time – 6 h).

Table 3
Benchmark dataset for the validation of PAR models, and results from the REST2, CPCR2, and Gueymard (1989) models for direct, diffuse and global PAR (in W/m^2) on a horizontal surface

Case #	Day[a]	CST[b]	Measured PAR			REST2 predicted			CPCR2 predicted			Gueymard (1989) predicted		
			Direct	Diffuse	Global	Direct	Diffuse	Global	Direct	Diffuse	Global	Direct	Diffuse	Global
15	11	0700	79.2	34.0	113.2	76.1	38.1	114.2	77.4	41.0	118.5	81.3	39.3	120.6
16	11	0920	280.1	49.0	329.2	272.8	55.0	327.8	258.1	71.5	329.5	270.5	66.7	337.2
18	11	1500	405.6	52.2	457.8	395.8	56.8	452.6	381.9	72.6	454.5	396.3	68.3	464.7
19	12	0730	124.7	38.8	163.5	119.3	43.3	162.6	108.4	53.6	162.0	115.8	50.7	166.4
20	12	0950	313.8	53.6	367.4	303.9	58.2	362.1	301.8	63.6	365.4	313.5	60.6	374.1
21	20	1400	335.5	89.3	424.8	324.7	89.0	413.7	312.6	105.1	417.6	330.6	99.2	429.8
22	22	0800	143.0	68.1	211.1	142.8	68.7	211.5	143.2	73.2	216.4	152.7	70.1	222.9
23	27	1300	333.4	115.0	448.4	325.7	113.2	438.8	322.5	123.8	446.2	342.1	118.2	460.4
25	28	0730	192.1	97.4	289.5	97.8	65.7	163.5	96.9	71.4	168.3	105.6	68.4	174.0
26	28	1800	62.0	49.9	111.9	60.0	50.9	111.0	61.9	54.4	116.2	67.3	52.3	119.6
27	29	0830	204.0	62.4	266.3	198.3	64.9	263.2	195.4	71.7	267.1	207.0	68.6	275.7
28	29	1230	396.3	69.1	465.4	383.4	71.2	454.6	380.3	79.4	459.7	396.7	76.5	473.2
Min			62.0	34.0	111.9	60.0	38.1	111.0	61.9	41.0	116.2	67.3	39.3	119.6
Max			405.6	115.0	465.4	395.8	113.2	454.6	381.9	123.8	459.7	396.7	118.2	473.2
Mean			231.4	62.2	293.6	225.0	64.6	289.6	220.0	73.4	293.5	231.6	69.9	301.5
Std. Dev.			126.9	22.3	138.5	123.2	20.3	134.7	120.1	22.3	135.0	124.4	21.2	138.7
MBD (%)						−2.7	−2.1	−1.4	−4.9	18.1	0.0	0.1	12.4	2.7
RMSD (%)						3.2	2.1	2.0	6.2	20.2	1.4	2.9	14.8	2.8

See Table 1 for atmospheric data in each case.
[a] Day of May 2003.
[b] Central Standard Time (Universal Time – 6 h).

benchmark for future studies. Table 2 compares the experimental determinations of illuminance to the predictions from REST2 and CPCR2. Similarly, Table 3 compares the measured PAR components to the predictions from REST2, CPCR2 and this author's original PAR model (Gueymard, 1989a). As already mentioned above for the irradiance performance results, REST2 offers much improvement over the older models for both illuminance and PAR, particularly with regard to diffuse radiation.

It is of course desirable to generalize these results through a full-fledged validation exercise, using data for various sites in widely different climates. Such an elaborate performance assessment study, similar in scope to that already done for DNI only (Gueymard, 2003b), and involving various BSRN datasets, is underway and will be reported soon. Preliminary results indicate that no existing broadband model of the literature approaches the accuracy of REST2, as far as the prediction of diffuse and global irradiance is concerned. For direct irradiance, REST2 is also a top performer, on par with REST and MLWT2. The excellent results of the three models just mentioned can be related to the fact that none of them uses empirical data in their algorithm.

6. Conclusions

The high-performance REST2 model is developed using transmittance parameterizations based on the SMARTS spectral model, separately for two broad bands of the shortwave spectrum: the UV–vis band (0.29–0.70 μm), and the near-infrared band (0.70–4.0 μm).

The proposed model uses the two Ångström turbidity coefficients, α and β. They can be easily derived from current aerosol data generated by ground-based sunphotometer networks (e.g., AERONET), and are thus of "universal" availability. The model's aerosol parameterization uses the concept of an effective aerosol wavelength along with Ångström's classic equation to improve accuracy.

Preliminary performance assessment results are presented, using a reference dataset. It is constituted of sophisticated measurements of clear-sky direct and diffuse irradiance, as well as simultaneous measurements of various atmospheric constituents (particularly aerosols), performed at the ARM-SGP site of Billings, Oklahoma during the Aerosol Intensive Observation Period of May 2003. These exceptional measurements constitute the first known modern benchmark dataset specifically assembled to test radiation models using the radiative closure method. By comparing the measured irradiances in this dataset to REST2's predictions it is demonstrated that the latter's average error is within the uncertainty of the best radiometric experimental procedures currently deployed. It can therefore be concluded that, under cloudless conditions, it is equivalent to measure irradiance with the best radiometers or to calculate irradiance with REST2 at any site where good sunphotometric data are available.

A turbidity-dependent parameterization of the ratio of illuminance to UV–vis irradiance is also proposed to obtain clear-sky illuminance and PAR, which can be very useful in various applications of the built and natural environments. The effect of turbidity is shown to be extremely significant on broadband irradiance, but even more so on PAR irradiance and illuminance. Preliminary validation results, using a part of the ARM-SGP benchmark dataset, confirm the accuracy of the REST2 predictions for illuminance and PAR under cloudless skies.

Acknowledgements

The development of REST2 was financially supported in part by the National Renewable Energy Laboratory. The AIOP experiment was made possible through the financial support of the U.S. Department of Energy's Atmospheric Radiation Measurement Program.

Appendix 1. Details on broadband irradiance calculations

- Transmittances, Band 1 (see also Eqs. (6) and (7))

$$T_{R1} = (1 + 1.8169m'_R - 0.033454m'^2_R)/(1 + 2.063m'_R + 0.31978m'^2_R)$$

$$T_{g1} = (1 + 0.95885m'_R + 0.012871m'^2_R)/(1 + 0.96321m'_R + 0.015455m'^2_R)$$

$$T_{o1} = (1 + f_1 m_o + f_2 m_o^2)/(1 + f_3 m_o)$$

$$f_1 = u_o(10.979 - 8.5421u_o)/(1 + 2.0115u_o + 40.189u_o^2)$$

$$f_2 = u_o(-0.027589 - 0.005138u_o)/(1 - 2.4857u_o + 13.942u_o^2)$$

$$f_3 = u_o(10.995 - 5.5001u_o)/(1 + 1.6784u_o + 42.406u_o^2)$$

$$T_{n1} = Min[1, (1 + g_1 m_w + g_2 m_w^2)/(1 + g_3 m_w)]$$

$$g_1 = (0.17499 + 41.654u_n - 2146.4u_n^2)/(1 + 22295.0u_n^2)$$

$$g_2 = u_n(-1.2134 + 59.324u_n)/(1 + 8847.8u_n^2)$$

$$g_3 = (0.17499 + 61.658u_n + 9196.4u_n^2)/(1 + 74109.0u_n^2)$$

$$T_{w1} = (1 + h_1 m_w)/(1 + h_2 m_w)$$

$$h_1 = w(0.065445 + 0.00029901w)/(1 + 1.2728w)$$

$$h_2 = w(0.065687 + 0.0013218w)/(1 + 1.2008w)$$

$$m'_R = m_R p/1013.25$$

- Transmittances, Band 2 (see also Eqs. (6) and (7))

$$T_{R2} = (1 - 0.010394m'_R)/(1 - 0.00011042m'^2_R)$$

$$T_{g2} = (1 + 0.27284m'_R - 0.00063699m'^2_R)/(1 + 0.30306m'_R)$$

$$T_{o2} = 1$$

$$T_{n2} = 1$$

$$T_{w2} = \left(1 + c_1 m_w + c_2 m_w^2\right)/\left(1 + c_3 m_w + c_4 m_w^2\right)$$

$$c_1 = w(19.566 - 1.6506w + 1.0672w^2) / (1 + 5.4248w + 1.6005w^2)$$

$$c_2 = w(0.50158 - 0.14732w + 0.047584w^2) / (1 + 1.1811w + 1.0699w^2)$$

$$c_3 = w(21.286 - 0.39232w + 1.2692w^2) / (1 + 4.8318w + 1.412w^2)$$

$$c_4 = w(0.70992 - 0.23155w + 0.096514w^2) / (1 + 0.44907w + 0.75425w^2)$$

- Effective aerosol wavelength, Band 1 (see also Eqs. (6) and (7))

$$\lambda_{e1} = (d_0 + d_1 u_a + d_2 u_a^2)/(1 + d_3 u_a^2)$$
$$d_0 = 0.57664 - 0.024743\alpha_1$$
$$d_1 = (0.093942 - 0.2269\alpha_1 + 0.12848\alpha_1^2)/(1 + 0.6418\alpha_1)$$
$$d_2 = (-0.093819 + 0.36668\alpha_1 - 0.12775\alpha_1^2)/(1 - 0.11651\alpha_1)$$
$$d_3 = \alpha_1(0.15232 - 0.087214\alpha_1 + 0.012664\alpha_1^2) / (1 - 0.90454\alpha_1 + 0.26167\alpha_1^2)$$

- Effective aerosol wavelength, Band 2 (see also Eqs. (6) and (7))

$$\lambda_{e2} = (e_0 + e_1 u_a + e_2 u_a^2)/(1 + e_3 u_a)$$
$$e_0 = (1.183 - 0.022989\alpha_2 + 0.020829\alpha_2^2)/(1 + 0.11133\alpha_2)$$
$$e_1 = (-0.50003 - 0.18329\alpha_2 + 0.23835\alpha_2^2)/(1 + 1.6756\alpha_2)$$
$$e_2 = (-0.50001 + 1.1414\alpha_2 + 0.0083589\alpha_2^2)/(1 + 11.168\alpha_2)$$
$$e_3 = (-0.70003 - 0.73587\alpha_2 + 0.51509\alpha_2^2)/(1 + 4.7665\alpha_2)$$

- Aerosol scattering correction factor, Band 1 (see Eq. (8))

$$F_1 = (g_0 + g_1\tau_{a1})/(1 + g_2\tau_{a1})$$
$$g_0 = (3.715 + 0.368m_a + 0.036294m_a^2)/(1 + 0.0009391m_a^2)$$
$$g_1 = (-0.164 - 0.72567m_a + 0.20701m_a^2)/(1 + 0.0019012m_a^2)$$
$$g_2 = (-0.052288 + 0.31902m_a + 0.17871m_a^2)/(1 + 0.0069592m_a^2)$$

- Aerosol scattering correction factor, Band 2 (see Eq. (8))

$$F_2 = (h_0 + h_1\tau_{a2})/(1 + h_2\tau_{a2})$$
$$h_0 = (3.4352 + 0.65267m_a + 0.00034328m_a^2)/(1 + 0.034388m_a^{1.5})$$
$$h_1 = (1.231 - 1.63853m_a + 0.20667m_a^2)/(1 + 0.1451m_a^{1.5})$$
$$h_2 = (0.8889 - 0.55063m_a + 0.50152m_a^2)/(1 + 0.14865m_a^{1.5})$$

- Sky albedo (for backscattered radiation, see Eq. (12))

$$\rho_{s1} = [0.13363 + 0.00077358\alpha_1 + \beta_1(0.37567 + 0.22946\alpha_1)/(1 - 0.10832\alpha_1)]/[1 + \beta_1(0.84057 + 0.68683\alpha_1)/(1 - 0.08158\alpha_1)]$$

$$\rho_{s2} = [0.010191 + 0.00085547\alpha_2 + \beta_2(0.14618 + 0.062758\alpha_2)/(1 - 0.19402\alpha_2)]/[1 + \beta_2(0.58101 + 0.17426\alpha_2)/(1 - 0.17586\alpha_2)]$$

Appendix 2. Details on illuminance and PAR calculations

- Illuminance calculations (see Eqs. (16) and (17))

$$m_{11} = \min(m_R, 11)$$
$$r_0 = 0.21437 + 0.021878m_{11} - 0.0037737m_{11}^2 + 0.00032857m_{11}^3 - 2.0789e-5m_{11}^4 + 6.7972e-7m_{11}^5$$
$$r_1 = 0.0040867 + 0.031571m_{11} + 0.0037634m_{11}^2 - 0.003198m_{11}^3 + 5.6847e-4m_{11}^4 - 2.7302e-5m_{11}^5$$
$$r_2 = -0.030167 + 0.013214m_{11} - 0.02685m_{11}^2 + 0.0076755m_{11}^3 - 9.3458e-4m_{11}^4 + 3.6227e-5m_{11}^5$$
$$r_3 = 0.67565 - 1.3181m_{11} + 0.87706m_{11}^2 - 0.1964m_{11}^3 + 0.022028m_{11}^4 - 0.000846m_{11}^5$$
$$s_0 = 0.21317 + 0.010589m_{11} - 0.0033043m_{11}^2 + 0.00041787m_{11}^3 - 2.7531e-5m_{11}^4 + 7.8175e-7m_{11}^5$$
$$s_1 = -0.19312 + 0.16898m_{11} - 0.072244m_{11}^2 + 0.013549m_{11}^3 - 9.2559e-4m_{11}^4 + 2.1105e-5m_{11}^5$$
$$s_2 = 0.034794 - 0.05233m_{11} + 0.023064m_{11}^2 - 0.0046273m_{11}^3 + 3.151e-4m_{11}^4 - 6.9504e-6m_{11}^5$$
$$s_3 = -0.81119 + 0.64533m_{11} - 0.2673m_{11}^2 + 0.048401m_{11}^3 - 0.0032342m_{11}^4 + 7.2347e-5m_{11}^5$$

- PAR calculations (see Eqs. (20) and (21))

$$m_{15} = \min(m_R, 15)$$
$$t_0 = (0.90227 + 0.29m_{15} + 0.22928m_{15}^2 - 0.0046842m_{15}^3)/(1 + 0.35474m_{15} + 0.19721m_{15}^2)$$
$$t_1 = (-0.10591 + 0.15416m_{15} - 0.048486m_{15}^2 + 0.0045932m_{15}^3)/(1 - 0.29044m_{15} + 0.026267m_{15}^2)$$
$$t_2 = (0.47291 - 0.44639m_{15} + 0.1414m_{15}^2 - 0.014978m_{15}^3)/(1 - 0.37798m_{15} + 0.052154m_{15}^2)$$
$$t_3 = (0.077407 + 0.18897m_{15} - 0.072869m_{15}^2 + 0.0068684m_{15}^3)/(1 - 0.25237m_{15} + 0.020566m_{15}^2)$$
$$v_0 = (0.82725 + 0.86015m_{15} + 0.007136m_{15}^2 + 0.00020289m_{15}^3)/(1 + 0.90358m_{15} + 0.015481m_{15}^2)$$
$$v_1 = (-0.089088 + 0.089226m_{15} - 0.021442m_{15}^2 + 0.0017054m_{15}^3)/(1 - 0.28573m_{15} + 0.024153m_{15}^2)$$
$$v_2 = (-0.05342 - 0.0034387m_{15} + 0.0050661m_{15}^2 - 0.00062569m_{15}^3)/(1 - 0.32663m_{15} + 0.029382m_{15}^2)$$
$$v_3 = (-0.17797 + 0.13134m_{15} - 0.030129m_{15}^2 + 0.0023343m_{15}^3)/(1 - 0.28211m_{15} + 0.023712m_{15}^2)$$

References

Alados-Arboledas, L. et al., 2000. Parametric models to estimate photosynthetically active radiation in Spain. Agric. For. Meteorol. 101, 187–201.

Battles, F.J. et al., 2000. Comparison of cloudless sky parameterizations of solar irradiance at various Spanish midlatitude locations. Theor. Appl. Climatol. 66, 81–93.

Cess, R.D. et al., 2000. Consistency tests applied to the measurement of total, direct, and diffuse shortwave radiation at the surface. J. Geophys. Res. 105D, 24881–24887.

Darula, S. et al., 2005. Reference luminous solar constant and solar luminance for illuminance calculations. Solar Energy 79, 559–565.

Gu, L. et al., 2002. Advantages of diffuse radiation for terrestrial ecosystem productivity. J. Geophys. Res. 107D. doi:10.1029/2001JD001242.

Gueymard, C.A., 1987. An anisotropic solar irradiance model for tilted surfaces and its comparison with selected engineering algorithms. Solar Energy 38, 367–386, Erratum, Solar Energy 40: 175 (1988).

Gueymard, C.A., 1989a. An atmospheric transmittance model for the calculation of the clear sky beam, diffuse and global photosynthetically active radiation. Agric. For. Meteorol. 45, 215–229.

Gueymard, C.A., 1989b. A two-band model for the calculation of clear sky solar irradiance, illuminance, and photosynthetically active radiation at the Earth's surface. Solar Energy 43, 253–265.

Gueymard, C.A., 1993a. Critical analysis and performance assessment of clear sky solar irradiance models using theoretical and measured data. Solar Energy 51, 121–138.

Gueymard, C.A., 1993b. Mathematically integrable parameterization of clear-sky beam and global irradiances and its use in daily irradiation applications. Solar Energy 50, 385–397.

Gueymard, C.A., 1995. The effect of cloudless atmospheres on the luminous efficacy of beam, diffuse, and global radiation. In: Campbell-Howe, R., Wilkins-Crowder, B. (Eds.), Proceedings of the Solar '95, Annual ASES Conference. American Solar Energy Society, Minneapolis, MN, pp. 188–193.

Gueymard, C.A., 2001. Parameterized transmittance model for direct beam and circumsolar spectral irradiance. Solar Energy 71, 325–346.

Gueymard, C.A., 2003a. Direct solar transmittance and irradiance predictions with broadband models. Part 1: Detailed theoretical performance assessment. Solar Energy 74, 355–379, Corrigendum: Solar Energy 76, 513 (2004).

Gueymard, C.A., 2003b. Direct solar transmittance and irradiance predictions with broadband models. Part 2: Validation with high-quality measurements. Solar Energy 74, 381–395, Corrigendum: Solar Energy 76, 515 (2004).

Gueymard, C.A., 2004a. The sun's total and spectral irradiance for solar energy applications and solar radiation models. Solar Energy 76, 423–452.

Gueymard, C.A., 2004b. High performance model for clear-sky irradiance and illuminance. Proceedings of the Solar 2004, Annual ASES Conference. American Solar Energy Society, Portland, OR.

Gueymard, C.A., 2005a. Interdisciplinary applications of a versatile spectral solar irradiance model: a review. Energy 30, 1551–1576.

Gueymard, C.A., 2005b. SMARTS Code, Version 2.9.5 User's Manual. Solar Consulting Services. Online PDF document, available from http://rredc.nrel.gov/solar/models/SMARTS/smarts_index.html.

Gueymard, C.A., in press. Prediction and validation of cloudless shortwave solar spectra incident on horizontal, tilted, or tracking surfaces. Solar Energy, doi:10.1016/j.solener.2007.04.007.

Gueymard, C.A., George, R., 2005. Gridded aerosol optical depth climatological datasets over continents for solar radiation modeling. Proceedings of the Solar World Congress. International Solar Energy Society, Orlando, FL.

Gueymard, C.A. et al., 2000. China's dust affects solar resource in the US: a case study. Proceedings of the Solar 2000, Annual ASES Conference. American Solar Energy Society, Madison, WI.

Holben, B.N. et al., 1998. AERONET – A federated instrument network and data archive for aerosol characterization. Remote Sens. Environ. 66, 1–16.

Ineichen, P., 2006. Comparison of eight clear sky broadband models against 16 independent data banks. Solar Energy 80, 468–478.

Lopez, G., Gueymard, C.A., 2007. Clear-sky solar luminous efficacy determination using artificial neural networks. Solar Energy 81, 929–939.

Michalsky, J. et al., 1999. Optimal measurement of surface shortwave irradiance using current instrumentation. J. Atmos. Ocean Technol. 16, 55–69.

Michalsky, J.J. et al., 2005. Toward the development of a diffuse horizontal shortwave irradiance working standard. J. Geophys. Res. 110D. doi:10.1029/2004JD005265.

Michalsky, J.J. et al., 2006. Shortwave radiative closure studies for clear skies during the Atmospheric Radiation Measurement 2003 Aerosol Intensive Observation Period. J. Geophys. Res. 111D. doi:10.1029/2005JD006341.

Michalsky, J.J. et al., 2007. A proposed working standard for the measurement of diffuse horizontal shortwave irradiance. J. Geophys. Res., 112D. doi:10.1029/2007JD008651.

Mueller, R.W. et al., 2004. Rethinking satellite based solar irradiance modelling – the SOLIS clear-sky module. Remote Sens. Environ. 91, 160–174.

Myers, D.R. et al., 2002. Recent progress in reducing the uncertainty in and improving pyranometer calibrations. Trans. ASME, J. Solar Energy Eng. 124, 44–50.

Olmo, F.J. et al., 2001. Performance reduction of solar irradiance parametric models due to limitations in required aerosol data: case of the CPCR2 model. Theor. Appl. Climatol. 69, 253–263.

Philipona, R., 2002. Underestimation of solar global and diffuse radiation measured at Earth's surface. J. Geophys. Res. 107D. doi:10.1029/2002JD002396.

Roderick, M.L. et al., 2001. On the direct effect of clouds and atmospheric particles on the productivity and structure of vegetation. Oecologia 129, 21–30.

Rothman, L.S. et al., 2005. The HITRAN 2004 molecular spectroscopic database. J. Quant. Spectrosc. Radiat. Transf. 96, 139–204.

Skartveit, A., Olseth, J.A., 1988. Some simple formulas for multiple Rayleigh scattered irradiance. Solar Energy 41, 19–20.